

Patterns of gas hydrate accumulation in mass transport deposits related to canyon activity: Example from Shenhu drilling area in the South China Sea

Chao Fu¹, Shengli Li^{1*}, Xinghe Yu¹, Jinqiang Liang², Zenggui Kuang², Yulin He², Lina Jin¹

¹ School of Energy Resources, China University of Geosciences, Beijing 100083, China

² Guangzhou Marine Geological Survey, China Geological Survey, Guangzhou 510760, China

Received 6 December 2017; accepted 26 March 2018

© Chinese Society for Oceanography and Springer-Verlag GmbH Germany, part of Springer Nature 2019

Abstract

Since 2017, a plenty of gas hydrates have been drilled in a new area of Shenhu, and good heterogeneity has been found throughout the spatial distribution of the reservoir. After distinguishing different sedimentary sequence types and matching their formation with slope deposition settings, this study proposes three mass transport deposit (MTD) patterns related to canyon activity that occurred contemporaneously or epigenetically with it: well preserved MTDs, MTDs eroded by canyon migration, and MTDs dislocated by contemporaneous faults. Based on seismic reflection characteristics, this study proposed methods of quantitatively analyzing sedimentary factors, such as measuring the turbidities flow rate in the canyon, and results are interpreted with respect to canyon activity. Combining the above parameters and their relationship with gas hydrate accumulation, fine-grained seals overlapping coarse MTDs reservoirs are found to be indispensable to gas hydrate accumulation, as they prevent the release of free gas. Based on grain size data of hydrate samples from drilling wells, multi-layered gas hydrate reservoirs capped by fine-grained sediments and overlapping mud show favorable hydrate-bearing prospects. The release of gas hydrates, however, is mostly caused by the lack of mud sealing in relation to canyon activity, such as turbidities flow erosion and contemporaneous fault breaking. Canyon migration with respect to MTDs may be the actual cause of erosion of overlapping syn-sedimentary layers, and high bottom flows may contribute to an increase in the release of free gas. It is believed that contemporaneous faults caused by unstable canyon walls may break the muddy over layers and decrease the accumulation pressure of gas hydrate bearing. Thus, according to the sedimentary characteristics of MTDs and the hydrate accumulation process, three responding accumulation or releasing patterns are proposed, which respond to the different types of MTDs distinguished above: a well-preserved MTD accumulation pattern; a canyon migration eroded MTD release pattern; and a micro-contemporaneous fault dislocated MTD release pattern.

Key words: South China Sea, gas hydrate, sedimentary characteristics, MTDs, hydrate responding pattern

Citation: Fu Chao, Li Shengli, Yu Xinghe, Liang Jinqiang, Kuang Zenggui, He Yulin, Jin Lina. 2019. Patterns of gas hydrate accumulation in mass transport deposits related to canyon activity: Example from Shenhu drilling area in the South China Sea. *Acta Oceanologica Sinica*, 38(5): 118–128, doi: 10.1007/s13131-019-1443-1

1 Introduction

Natural gas hydrates are quasi-ice crystalline compounds composed of water and natural gas that are formed in a low temperature and high-pressure environment (Holbrook et al., 1996). Former studies have shown that mass transport deposits (MTDs) are favorable reservoirs for gas hydrate accumulation (Wu et al., 2011; Yu et al., 2014). Complex hydrodynamic settings in slope regions and canyon activity migration science the Miocene have led to the development of many MTD types, which makes investigations into MTD preservation and corresponding gas hydrate accumulation patterns challenging (Yu et al., 2014; Riedel et al., 2013b).

If pore types are effective and suitable accumulation conditions are provided, such as suitable temperatures and pressures, it is believed that MTDs could enable gas accumulation and serve as potential reservoirs (Wu et al., 2011; Yu et al., 2014). In addition, many different deposition processes intervene with MTDs, and successive reworking lead to valuable gas hydrate accumulation patterns therein. For example, Scholz et al. (2012) and Riedel

et al. (2013a) analyzed seismic data and core samples from the Ullung Basin and found hydrate-bearing heterogeneity in different MTD reservoir types (Scholz et al., 2012; Riedel et al., 2013b). However, they also found extremely low gas hydrate saturation in a single MTD, but as it did not have a fine-grained seal bed they determined that gas hydrates mainly occur in multiple MTDs (multi-MTDs). Multi-MTDs create thick reservoirs and have good sealing conditions that are suitable for gas hydrate accumulation. Bangs et al. (2011) found variable bottom simulating reflections (BSR) between well-preserved MTDs where there was no later canyon activity reworking, and displaced one during study of the hydrate ridge in the Northwest Pacific in Western North America (Bangs et al., 2011). Nevertheless, the relationship between MTDs and hydrate accumulation has not been adequately defined and currently remains unclear.

The GMGS-3 drilling area (Fig. 1a) is located at the bottom of the northern slope of the South China Sea (SCS). Earlier research has studied the complex sedimentary setting and its depositional characteristics in the area (He et al., 2013; Chen et al., 2016). For

*Corresponding author, E-mail: slli@cugb.edu.cn

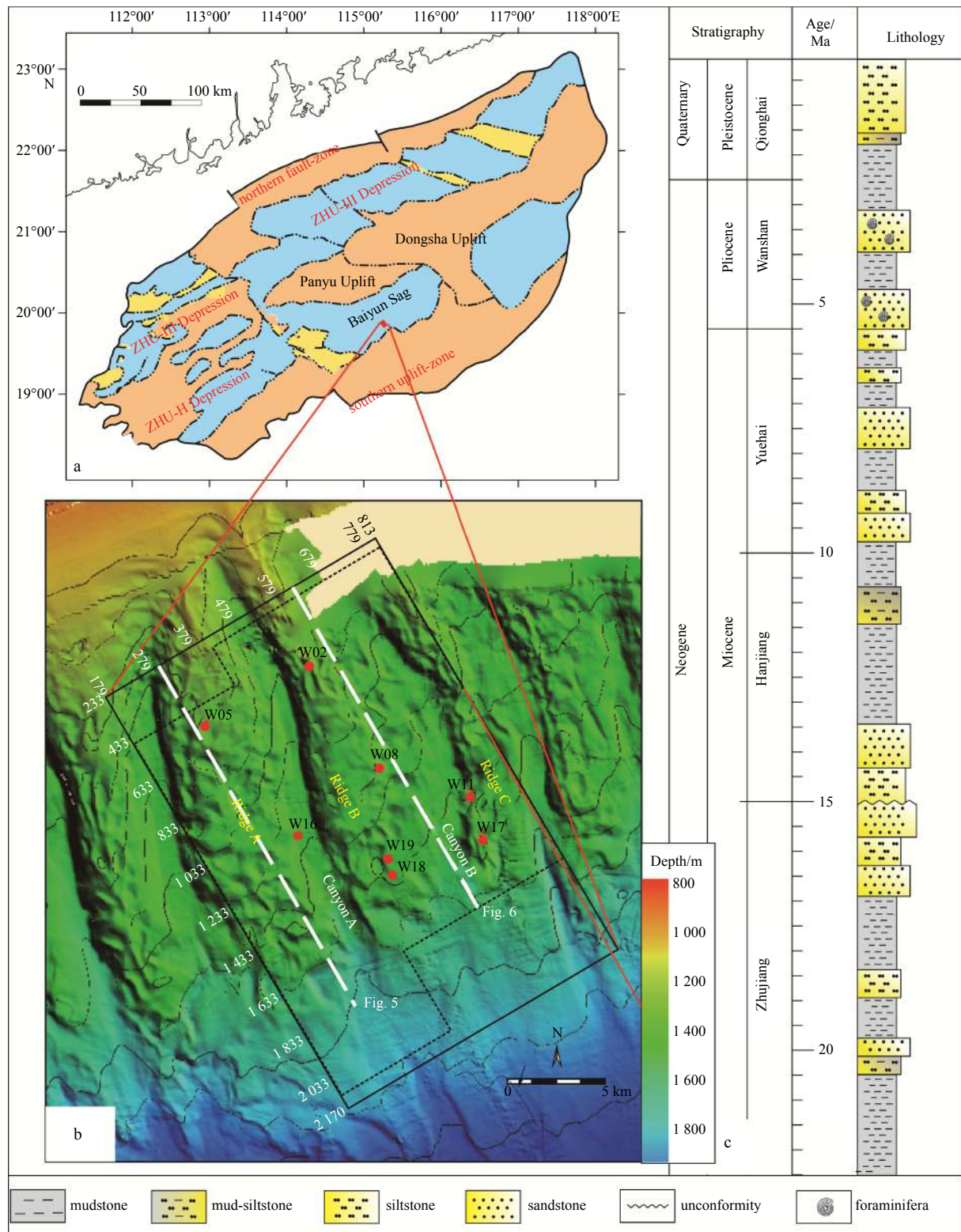


Fig. 1. Location of study area and integrated histogram. a. Tectonic units of Baiyun Sag and position of GMGS3; b. geomorphological map and well sites, water depth ranges from 800 m to 2 000 m, main topography includes ridges and valleys. Ridge areas are numbered from left to right: Ridge A, Ridge B, and Ridge C; and canyons are also numbered from left to right: Canyon A and Canyon B; and c. integrated histogram, from left to right: formation names of layers, chrono-stratigraphic age, main lithologies.

example, per studied sedimentary characteristics in the earlier drilling area of Shenhu (GMGS-1: location shown in Fig. 1) and found that MTDs could serve as an ideal gas hydrate reservoir

and that their classification can be based on topographical changes (Yu et al., 2014). From the perspective of bottom flow interaction and reworking, Gong et al. (2016) showed that the con-

tourites or bottom currents rebuild canyons lead to canyon migration, and that the intensity of the bottom flow may also act as an external mechanism for MTD formation. He classified MTDs into two types: normal MTDs and MTDs eroded by external turbidities flow. However, due to the lack of deep-water core samples from Shenhua, the characteristics of MTD reservoirs and their hydrate response patterns therein could not be clarified.

This study uses measurements of MTDs, such as thickness, distribution length, scale covered, sedimentary characteristics, and core-log-seismic integration analyses to categorize MTDs into three types in relation to canyon activity. Unidirectional canyon migration (UCM) and erosion of the canyon wall enabled the number of MTDs in the study area to be identified using 3D seismic data interpretation and attribute analyses. In addition, seismic facies were distinguished and their profiles interpreted, which enabled classification of MTDs into three types: (1) well-preserved MTDs, (2) MTDs eroded by canyon migration, and (3) MTDs dislocated by contemporaneous faults. An analysis of hydrate accumulation theory has led to the suggestion of three corresponding patterns, namely: (1) a well-preserved MTD accumulation pattern (such as the sandwich pattern, which has two layers of fine sediment beneath and above a coarse-grained reservoir and was introduced by Malinverno (2010) in the Cascadia margin); (2) a canyon-migration eroded MTD release pattern (such as the canyon pattern introduced by Boswell et al. (2012), in the Gulf of Mexico and Vadakkepuliyaambatta et al. (2015), in the Barents Sea, in which the decrease in heat flow and increase in the erosion rate in the canyon area was defined); and (3) a micro- contemporaneous faults dislocated MTD release pattern (which is determined in this study). Turbidites flow may lead to canyon wall erosion, which then causes sediments to become unstable; therefore, the above patterns may also form micro- contemporaneous faults. In each of these three patterns, a fine reservoir seal is found to be indispensable to hydrate accumulation and release. It is considered that the response patterns presented in this paper will enhance understanding of the relationship between MTD development and hydrate accumulation, and enable improved hydrate prediction in the high dip, angular, slope of passive continental margins (an area that facilitates MTD development).

This paper is organized as follows: the geological settings, methodologies, and data preparation are firstly presented to provide a background to this study. The different types of MTDs are then identified through seismic-log-core integration analysis, and MTD hydrate-bearing patterns are constructed in relation to the hydrate distribution area. Finally, factors impacting accumulation patterns are discussed.

2 Geological setting

The new drilling area in Shenhua is located in the central section of the northern slope of the SCS and constitutes a deep-sea sedimentary area of the Baiyun Sag in the southern Zhujiang (Pearl) River Mouth Basin (ZRMBS) (115°10' to 115°20'E) (Fig. 1a). The ZRMBS is a Cenozoic sedimentary basin that has experienced three tectonic stages since the Paleogene, namely a rift stage during the Paleocene to the early Oligocene, a transition in the late Oligocene, and a depression during the early Miocene to Quaternary (Han et al., 2016). During the late Oligocene to early Miocene, "Baiyun" movement (belonging to the latest tectonic stage) caused the Zhujiang (Pearl) River Estuary shelf slope to break and drift northwards, thereby becoming the depositional center of the Baiyun Sag; it then evolved into a deep-water slope environment (Clift et al., 2002; Han et al., 2016).

onment (Clift et al., 2002; Han et al., 2016).

Han et al. (2016) proposed the following: sea levels in SCS have been rising continuously since the late Miocene, there has been an increase in the extent of SCS transgression, the seaward progress of the Zhujiang River Estuary shelf delta is limited, and there has been a simultaneous and significant northward migration of the sedimentation process. The Shenhua area lies in the southern deep-water area of the ZRMBS (Fig. 1b), which is far from the provenance from the Zhujiang River; therefore, transported sediment is relatively small and fine-grained (Li et al., 2015).

The main well sites studied here are distributed in the canyon area (well sites shown in Fig. 1b). The canyon is located in the central part of the Baiyun Sag and lies mostly in a NNW direction (Fig. 1b). The drilled hydrate reservoirs are mainly composed of hemipelagic foraminifera, and fine silt and shale in the Yuehai and Wanshan Formations (Fig. 1c) (Wang et al., 2014; Sha et al., 2015). Based on multi-beam submarine topography data (Fig. 1b), the upper part of the slope is found to mainly have an asymmetric V-shaped or symmetric U-shaped structure, whereas the lower part of the slope is relatively flat. The study area is located at depths of 800–2 000 m, and there is a large gradient throughout the entire study area, with a maximum gradient of 3°.

The modern ocean circulation in the SCS is mainly controlled by semi-enclosed basin physiography and can be divided into seasonal surface-water circulation (<350 m), intermediate water circulation resulting from North Pacific intermediate water (NPIW; 350–1 350 m), and deep-water circulation associated with North Pacific deep water (>1 350 m). Along-slope bottom (contour) currents generally involve significant water masses at certain bathymetric depth ranges that persist for very long time intervals. It is therefore considered that the bottom currents associated with intermediate water circulation resulting from the NPIW (NPIW-BCs) are most likely to have had a profound influence on the development of the unidirectional migrating deep-water channels that are studied here, which are located primarily in water depths ranging from 500–1 300 m.

3 Data and methodology

Pseudo-three-dimensional (3D) survey data were acquired by GMGS between 2008 and 2009, using a frequency of 65 Hz and a sampling interval of 1 ms over an area measuring approximately 15 km by 25 km. To accurately describe the hydrate-bearing layers, time windows were set at 3 ms per slice. Log data were acquired by Fugro and processed by Schlumberger in 2015. Data acquired by the Guangzhou Marine Geological Survey (GMGS)-3 include the use of natural gamma-rays, gamma density, resistivity, and sonic velocity. *In situ* core samples in the target layers were taken using two kinds of pressure-core-barre tools (FPC, PCTB) and three non-pressure-core-barre tools (FHPC, FMCB, FXMCB). Due to the salt extraction effect of hydrate, the value of the resistivity log was abnormally high in the target layers (Riedel et al., 2013a). The grain size was measured using Mastersizer[®] 2000 with a laser particle size analyzer (SYE209) in Well11 (W11), Well17 (W17), Well18 (W18), and Well 19 (W19).

Studies of variable MTD development patterns are based on the integration of seismic data, log data, and core analyses. Mitchum (1977) first proposed the seismic facies analysis methodology to study sedimentary characteristics; this is based on the morphology of seismic reflectors, reflection of the seismic boundary, and the contact relation between different seismic facies (see the seismic facies listed in Fig. 2).



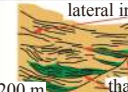
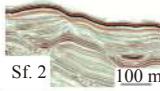

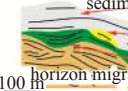
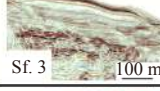
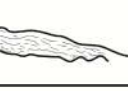
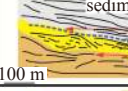



		Semitic example	Semitic interpre.	Sf. reflection	Depositional characteristics
Concave	incline concave Sf.	 Sf. 1 200 m		low amplitude lateral migration reflections	 lateral inclined deposit basal erosional discontinuities thalweg deposit
	horizon concave Sf.	 Sf. 2 100 m		moderate amplitude horizon migration reflections	 sedimentary wave MTDs horizon migration canyon
Chaotic	mound chaotic Sf.	 Sf. 3 100 m		high amplitude random reflections	 sedimentary wave BSR MTDs
	chimney chaotic Sf.	 Sf. 4 50 m		high amplitude random reflections	 BSR gas chimney

Fig. 2. Characteristics of seismic facies (Sf.) with respect to contact relationship with seismic events. Given the inner character of seismic packages its boundary, seismic facies are divided into two types, concave and chaotic facies. Seismic facies are then divided into four types, numbered from Sf. 1 to Sf. 4.

In this study, the turbidities flow rate in the canyon was calculated using the following four steps: (1) dividing the seismic data into three slices (Figs 3a–c: 1 500 ms, 2 000 ms and 2 500 ms); (2) decompacting the surface of each sequence using 2DMove software and reconstructing the paleo-geomorphology of each slice (Figs 3a–c); (3) calibrating the depositional rate of each well (W02, W05, W08, W16, W17, W18, W19) using the equation: $v_s = 4.2\Phi - 0.2$, where Φ is the corresponding grain size (see the Rose graph in Fig. 3); and (4) calibrating each well, subtracting the thickness of adjacent slices, then calculating the turbidities flow rate with well-integrated data.

The methodology used to distinguish hydrates is based on

seismic reflection and corresponding log calibration. Using core samples from Wells W11, W17, W18 and W19 (Fig. 4) and their corresponding resistance curves (Rt) at depths of 40–100 m and >120 m (Fig. 4), the hydrate saturation of the bearing layers was calculated (Table 1) using Archie's formula (the empirical parameter is determined as ' a ' = 1.0 and ' m ' = 1.8 (unconsolidated), through *in situ* pore turbidities flow salinity data).

4 Seismic geomorphology and recognition of MTDs

4.1 Seismic facies analysis

With respect to studies of 3-D seismic volume work conduc-

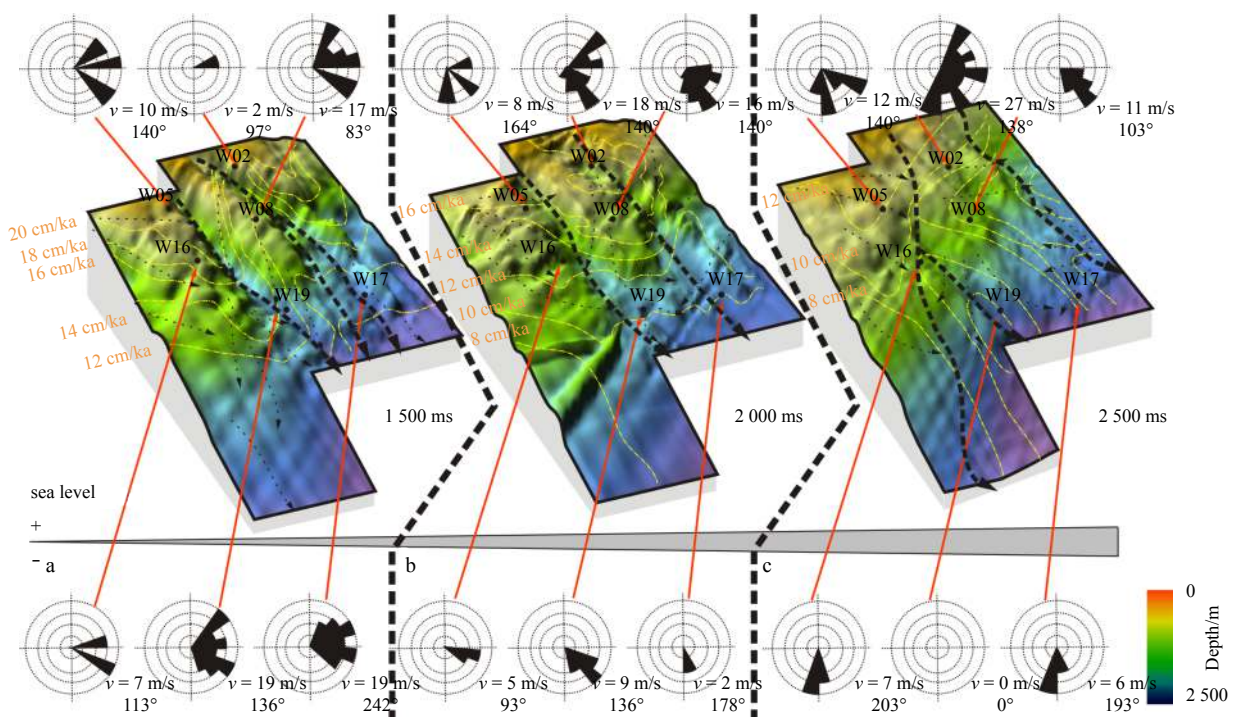


Fig. 3. Sedimentary and turbidities flow rates in study area. Paleo-geomorphology of different geological times since 11.8 Ma, from bottom to top: top of 1 000 ms (a), top of 1 250 ms (b), and top of 1 500 ms (c). Yellow dotted-line refers to changes in turbidities flow rate. Rose-diagram represents the flow rate and direction of turbidities flows in the channel.

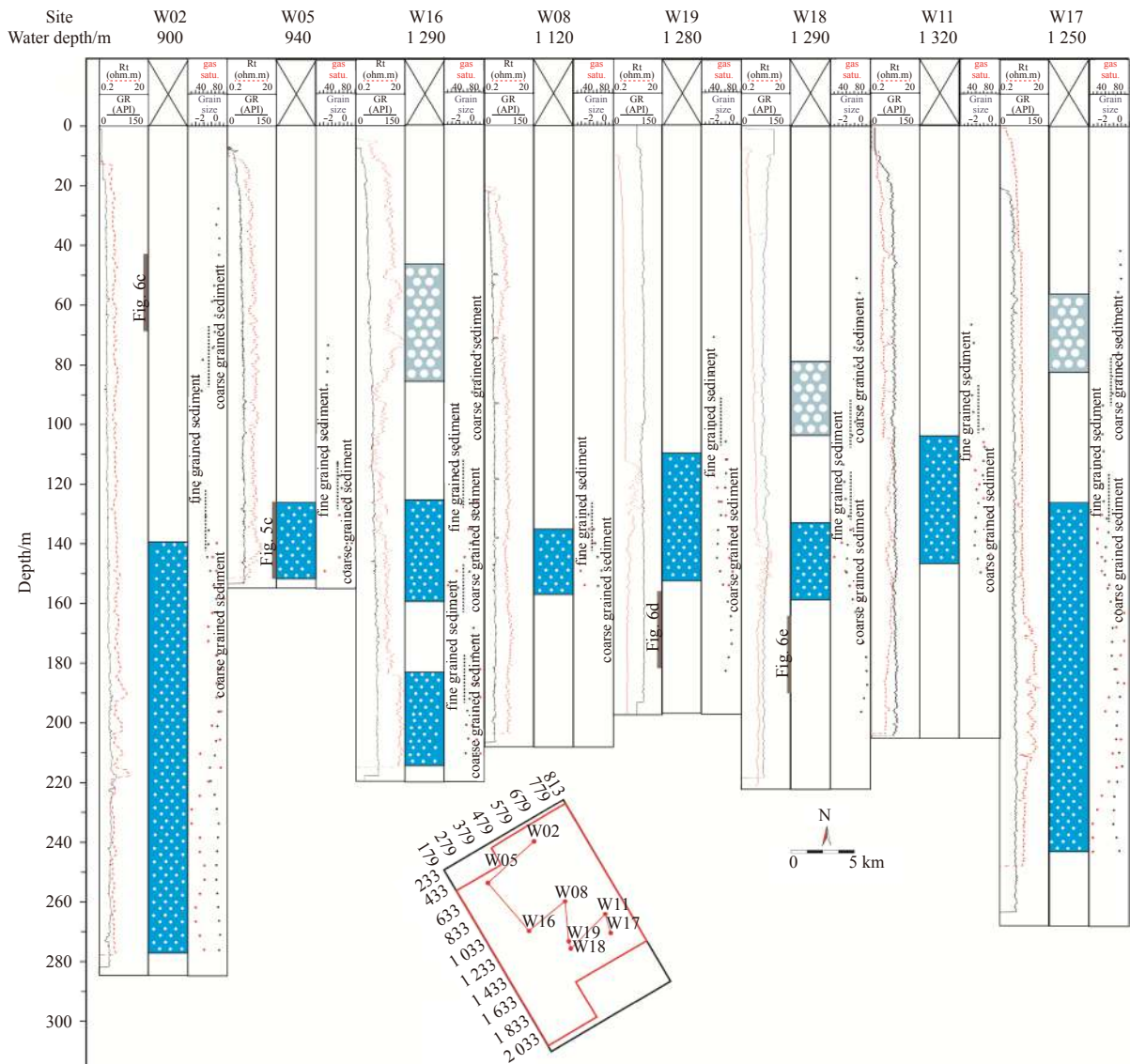


Fig. 4. Log data of GMGS-3 and corresponding saturation. Red dotted-line represents GR and black active line resistivity; hydrate layers interpreted in the middle are based on the Archie formula and core sample observation; gain size and hydrate saturation on the right are the result of calculations, which show that fine-grained layers exist above and beneath the coarse-grain layers.

Table 1. Saturation distribution of different wells

Well	Hydrate layers	Accumulation state	Crack width and developed density	Hydrate saturations
W11	14.94–19	fracture filling	development of subtle cracks, average width 2 mm	0.2–0.4
	27–33.98	fracture filling	development of subtle cracks, average width 2 mm	0.2–0.4
W17	104–122.3	fine grain filling	non-development of crack, soup structure	0.6–0.7
	54–65.49	fracture filling	development of subtle cracks, average width 3 mm	0.35–0.5
W18	155.44–203.75	fine grain filling	non-development of crack, soup structure	>0.8
	117.44–130	fine grain filling	development of subtle cracks, average width 2 mm	0.4–0.5
W19	130–163.5	fine grain filling	development of subtle cracks, average width 2 mm	0.4–0.5
	53.08–59.08	fracture filling	development of subtle cracks, average width 2 mm	<0.3

ted in the study area, and according to seismic reflection results and strengths and weaknesses, the seismic facies can be divided into two types: concave facies and chaotic facies (Fig. 2). Concave facies are characterized by down lap reflector packages (Fig. 2: concave) and chaotic facies are characterized by discontinuous and disorderly reflector packages (Fig. 2: radom); these are fur-

ther described as follows.

Concave facies: Based on the external geometric morphology of a seismic reflection, concave facies can be divided into lateral-concave facies (Sf. 1) and horizontal-concave facies (Sf. 2). Lateral-concave facies (Sf. 1) are characterized by discontinuous reflector packages, high-amplitude reflections, and unidirectional

migration of the truncated surface (reflector packages undergo upward migration following aggrading), which can be explained as being the directional migration of the canyon (Wang et al., 2014). Horizontal-concave facies (Sf. 2) have continuous reflector packages, low-amplitudes, and show horizontal migration of the truncated surface.

Chaotic facies: chaotic facies present as discontinuous internal seismic reflectors and can be divided into mound-chaotic (Sf. 3) and chimney-chaotic (Sf. 4) facies. Mound-chaotic facies (Sf. 3) have a chaotic internal reflector package with a high amplitude and a mound reflection boundary, representing MTDs; but chimney-chaotic facies (Sf. 4) also have a chaotic internal reflector package. The chimney-shaped reflection boundary is thought to be an abnormal reflection caused by the upward movement of free gas from the bottom.

4.2 Seismic profile analysis

This paper refers to two NNW-direction profiles through well sections (inline 300 and inline 500) that were selected to study the vertical MTD distribution of sedimentary facies. Positions of the profiles are shown in Fig. 1b, where the section indicates 20 km of inline direction and 15 km of crossline direction.

Profile A (Fig. 5: inline 300) is located in the western part of the study area (profile position is shown in Fig. 1b) and passes through Well W05. Use of 1 250–1 750 ms distinguishes mound-chaotic facies (Sf. 4), and two types can be identified in the profile: (1) mound-chaotic facies (Fig. 5c) have a continuous seismic

facies boundary, cluttered internal seismic event, and high attributes, while the seismic event of the upper overburden is not significantly broken; (2) mound-chaotic facies (Fig. 5d) have an indistinct facies boundary, and the seismic event of the upper overburden has an obvious dislocation.

Profile B (Fig. 6: inline 500) is located in the east of the study area (profile position is shown in Fig. 1), passes through wells W02, W08, W19, and W18, and mainly through Canyon A and Ridge B. Use of 1 250–1 500 ms enables identification of three types of mound-chaotic facies in the profile: (1) MTDs (Fig. 6c) are influenced by the effect of erosion and have a serious seismic erosion surface with a high amplitude; (2) chaotic facies (Fig. 6d) and (3) fault lines of mound-chaotic facies (Fig. 6e) are also development with a maximum length of more than 100 m and a small overall thickness.

5 Corresponding MTD classification and sedimentary characteristics

5.1 Type I MTDs

Well-preserved MTDs developed along the unstable slope setting, and most developed along slope-breaks, such as within the southern Cretan Sea, Peri-Adriatic Sea, and SCS (Strozyk et al., 2009; Di Celma, 2011; Zhou et al., 2015). Profile B, shown in Fig. 6, shows that multi-layer developed over the well-preserved MTDs, meaning the. Combined with the corresponding hydrate-bearing core sample in Fig. 4, W11, W17, W18 and W19

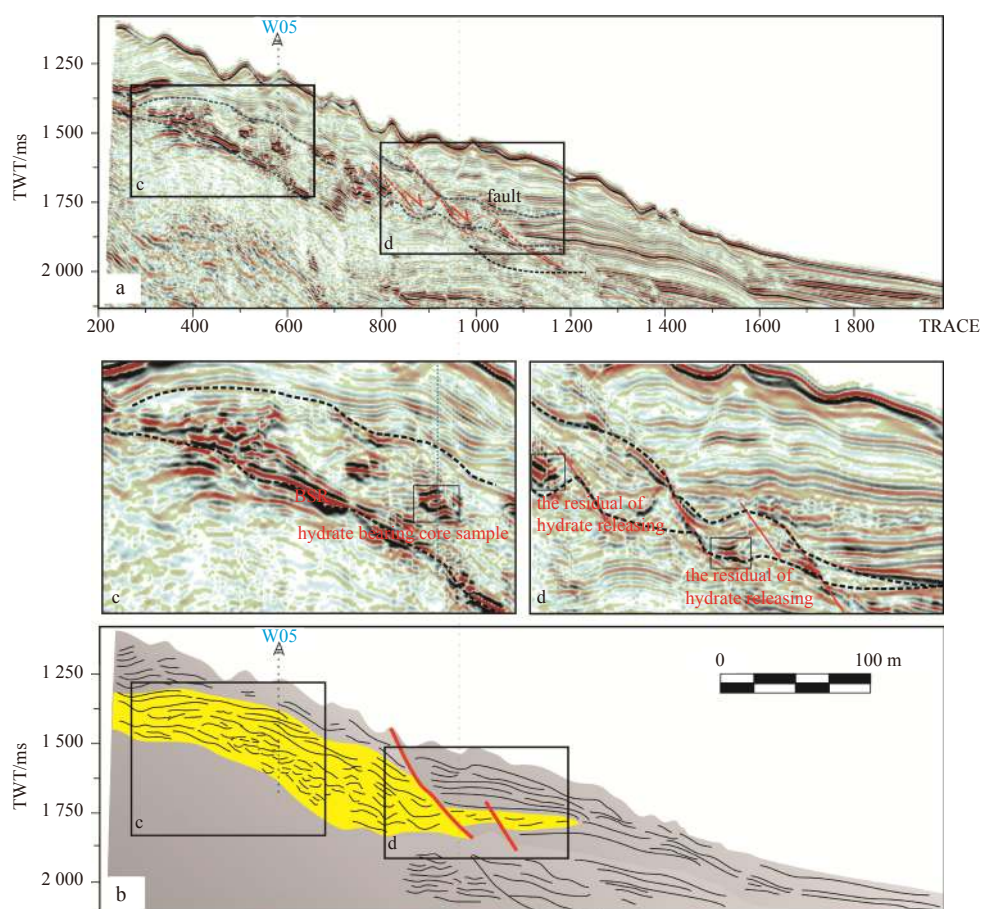


Fig. 5. Seismic Section A passing through W05 (select inline 300); the lower part is the sedimentary section used to analyze the internal structure of a seismic event. c and d show the enlarged MTD of the seismic profile; c shows a well-preserved MTD; and d shows an MTD broken by micro-contemporaneous faults, which have not dislocated the upper fine-grained layer.

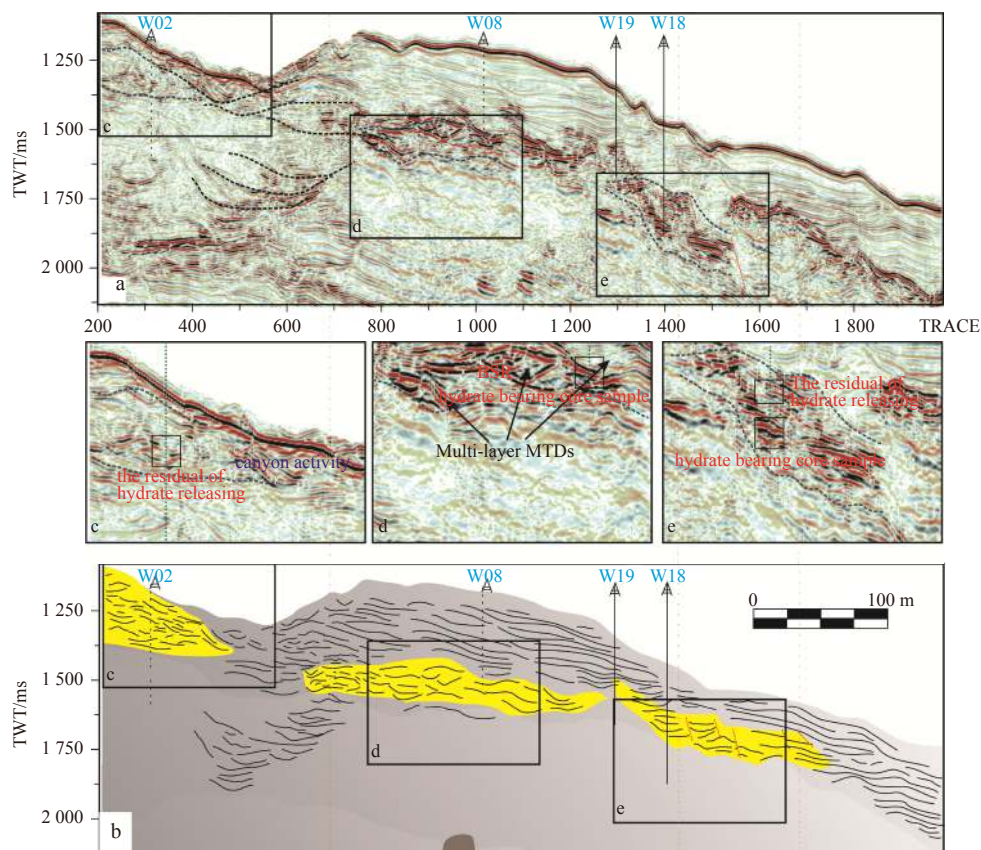


Fig. 6. Seismic Section B passing through W08, W18 and W19 (select inline 500); the lower part is the sedimentary section used to analyze the internal structure of a seismic event. c, d and e show the enlarged MTD of the seismic profile; c shows MTDs eroded by the lateral canyon; d shows multi- layers MTDs; and e shows an MTD broken by micro- contemporaneous faults.

show rhythmic variations in MTD grain sizes, which can be referred to as “sandwich layers”.

5.2 Type II MTDs

Based on interpretation of the seismic profile shown in Fig. 6c above, it appears that most Type II MTDs developed upstream of Type I MTDs and therefore underwent more intensive and complex reworking by the flow. Alsop et al. (2016) showed that sedimentation and turbidities flow rates are important factors in MTD formation. Meanwhile, the fine-grained layers over Type II MTDs are mostly reworked during later turbidities flow erosion.

5.3 Type III MTDs

Based on the seismic profiles shown in Figs 5b, 6c and the interpretation above, Type III MTDs are developed over a larger region. However, most are developed in the downstream slope-bottom of Type I MTDs (Fig. 7a: Type III). Micro-contemporaneous faults may have developed in relation to the following factors: free gas flow and a decrease in cementation between particles, differential settlement, and tectonic movement. For example, due to tectonic movement, the feet of Ridges A and B are formed in areas that have undergone rapid geomorphic basement changes (the dip angle changes from 5° to 2°–4° per km). Contemporaneous faults are formed when the shear stress is larger than the shearing strength of the MTD; when the shear force of MTDs increases, the slump in progress restarts. Thus, contemporaneous faults may dislocate the above fine-grained over-layers (as in profiles Figs 5d, 6e).

6 Corresponding MTD hydrate-bearing patterns

6.1 Hydrate reflection characteristics

Hydrate saturation in each well was determined by the pressure release in the core through in-situ observations of the four core wells (W11, W18, W17 and W19) (Table 1). However, due to the restricted number of wells in the GMGS-3 area and other parameters, and therefore the lack of data for the drilling area, it was necessary to study and evaluate the seismic reflection characteristics of the hydrate-bearing layers (Table 2) to determine the hydrate distribution. From a comparison between original sections and synthetic seismograms from high-resistivity regions (Wang et al., 2011), the bottom of the hydrate-bearing layer (BGHSZ) in GMGS-3 was found to be developed with an amplitude anomaly due to free gas, and this was found to decrease the P-velocity. Nevertheless, the BGHSZ shows a blank reflection band in the seismic profiles (Horozal et al., 2015), and the hydrate response in the BSR indicates skewed reflection characteristics and exhibits an amplitude anomaly.

6.2 Response pattern of hydrate-bearing MTDs

The progress of gas hydrate accumulation is controlled by many sediment-related factors, such as grain size, sand content, porosity, and turbidities flow rate (Wood et al., 2008; Behseresht and Bryant, 2012). The combination of a hydrate-bearing core sample and hydrate accumulation system, where the above MTDs types could be projected into three patterns, to respond to hydrate accumulation/ released (Wu et al., 2011; Sha et al., 2015;

Table 2. BSR reflection characteristics of hydrate-bearing layers in each well

Site	BSR reflection characteristics	Type	Time	Depth range/m	Lithology	C1/C2
W11	moderate amplitude, low continuity, appearance BGHSZ	W/S	late Miocene	94–399 (from core sample)	silt stone	200
W17	high amplitude, low continuity, appearance BGHSZ	S	late Miocene	94–399 (from core sample)	silt stone	180
W18	high amplitude, low continuity, appearance BGHSZ	S	late Miocene	160–345 (from core sample)	silt stone	200
W19	low amplitude, low continuity, appearance BGHSZ	S	late Miocene	160–345 (from core sample)	silt stone	250

Vadakepuliambatta et al., 2015) (AM.1, RM.2 and RM.2) (Fig. 8), and these are explained as follows.

6.2.1 Well-preserved MTDs accumulation pattern

Type I MTDs shown in seismic profiles (Figs 5a, 6b) are well-preserved MTDs that have developed with a complete sedimentary structure, namely crown cracks, basal shear surface, and toe thrust (Fig. 7a2). These kinds of MTDs develop with moderate thicknesses (40–80 m per MTDs) and have moderate spans (100–200 m² per MTDs). The continuous seismic events occurring above MTDs can be interpreted by the fine layer, serving as a seal and cap for free gas. Based on hydrate calculations and the volume of MTD development (as shown in Fig. 7a3) Type I MTDs

have good gas hydrate reflections.

The well-preserved MTD accumulation pattern can be simplified and referred to as a “sandwich accumulation pattern” (Fig. 8a3). As shown by the porosity curve in Fig. 8a3, hydrate-bearing sand and fine mud mutually overlaps in Type I MTDs. During gas hydrate resource appraisal, the following are considered: the thermal genetic gas supply, reaction time, effective migration, reservoir litho-facies, effective porosity, and gas hydrate stability zone. This type of sandwich pattern (AM.1) not only provides sufficient reaction time for the formation of clathrate hydrates but also provides sufficient porosity for hydrates. Therefore, AM.1 types serve as reservoirs for fine-grained filling hydrate under suitable temperatures and pressures.

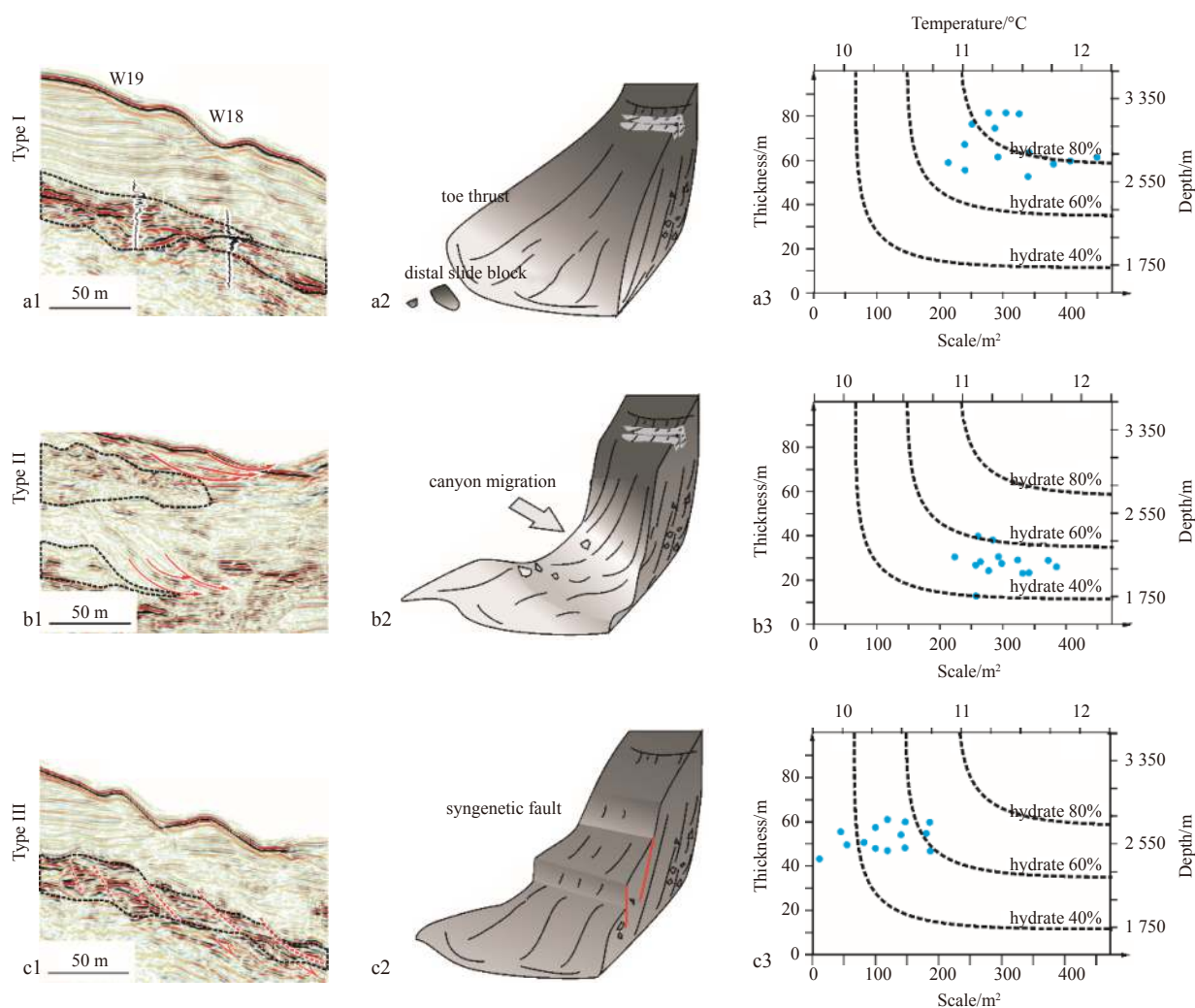


Fig. 7. Different types of MTDs distinguished in the study relating to gas hydrate accumulation; a1, a2 and a3 are seismic profiles showing different types of MTD-bearing hydrates; b1, b2 and b3 are sedimentary patterns of the above MTDs; c1, c2 and c3 are thickness and scale of MTD statistics obtained from the seismic profile; and the blue scatter shows hydrate saturation bearing in variable types of MTDs.

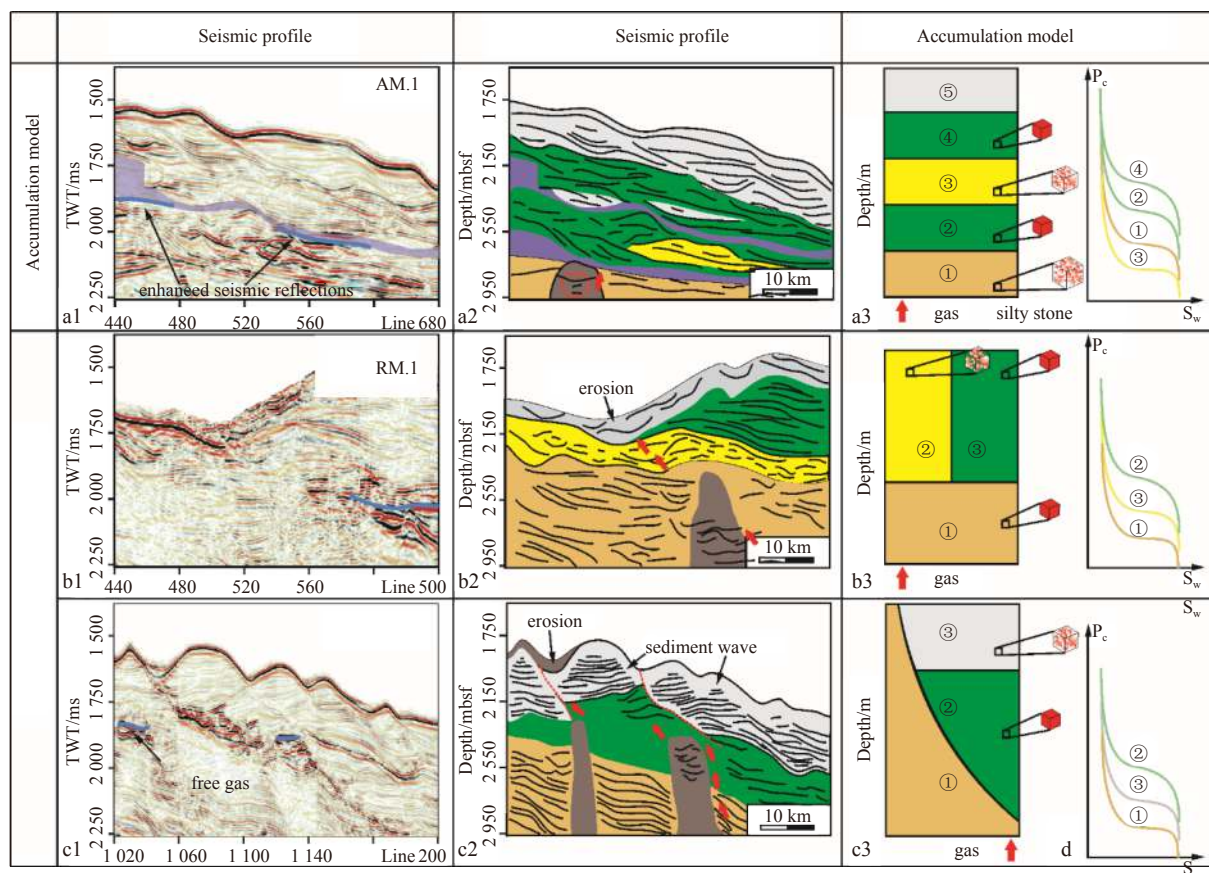


Fig. 8. Three response models for hydrate accumulation. a1, a2 and a3 seismic profiles selected in the study area, where the purple line is the BSR; b1, b2 and b3 sedimentary interpretations of seismic profile where the yellow area represents MTD development; c1, c2 and c3 response models with porosity curve on the right. The red cube represents grain sizes in different layers. mbsf represents meters below sea floor.

6.2.2 Canyon migration eroded MTD release pattern

In Type II MTDs (shown in the seismic profile of Fig. 6a), canyon migration eroded MTDs developed with an incomplete depositional structure (Fig. 7a2), small thicknesses (20–40 m per MTD) and on a moderate scale (100–200 m² per MTD). Despite not procuring a drilling sample, the type of BRS reflection and low amplitude (Profile B and Well 2 shown in Fig. 6) prove that these MTDs have low saturation levels (Fig. 7b3). When UCM erosion has occurred and the MTD structure has been broken, a release pattern (RM. 1) is likely to form. The fine layer overlapping the coarse hydrate-bearing siltstone is also eroded. In addition, with respect to the high turbidities flow rate caused by turbidities passing (the turbidities flow rate is shown in Fig. 3), the release of free gas leads to a decrease in gas saturation in these reservoirs. Thus, as shown by RM.2 in Fig. 8b3, free gas migrates from the gas chimney and is easily released into the sea water. In addition, there is insufficient reaction time, and excess turbidities flowing in the canyon may change the heat flux distribution and geochemistry, thereby influencing hydrate accumulation.

6.2.3 Micro- contemporaneous faults dislocated MTD release pattern

Type III MTDs shown in the seismic profile (Figs 5c and 6c) are related to micro-contemporaneous faults that have dislocated MTDs (Fig. 7c2). These kinds of MTDs develop with moderate thicknesses (20–40 m per MTD) and on a small scale (<100 m²

per MTD). The seismic amplitude is less intense than that of Type I, which implies that Type III MTDs have a lower hydrate saturation than Type I MTDs (Fig. 7c3).

A previous study showed that normal faults can not only break the primary structure but can also serve as a pathway for free gas migration (Lee et al., 2012; Jeong et al., 2014). Meanwhile, normal faults provide available space for hydrates and can also serve as reservoirs for fracture-filling hydrates.

Therefore, as shown in Figs 8a3 and c3, fault slip may be a key factor for gas accumulation. If the slip distance is less than half the thickness of the MTD, it is classified as AM.1, and if not it is classified as RM. 2.

The three different MTD types shown above have different hydrate responses, and all patterns can be summarized into litho-facies assemblages. If fine layers act as a seal for the hydrate reservoir, free gas is not easily released and hydrate accumulation progresses easily. Thus, in a fine canyon system, UCM and uneven subsidence of the canyon floor may be the main causes of broken MTD reservoirs in the Shenhu new drilling area.

7 Factors impacting gas hydrate bearing-MTDs

The hydrate accumulation pattern in Fig. 8 considers both porosity and the fine-grain seal above the MTD. In addition, according to the hydrate accumulation system, the temperature, pressure, and gas source also have an impact on accumulation.

7.1 Effect of pressure-temperature

Hydrate accumulation pressure is comprised of hydrostatic pressure and litho-static pressure. In the drilling area, the water depth ranges from 820 m to 1 445 m. On the northern slope of the SCS, values of heat flow range from 6 to 191 mW/m² with an average value of 76 mW/m² (Shi et al., 2003; Zhang et al., 2011).

However, differences between the preservation settings of MTDs may lead to considerable heterogeneity in the heat flow. According to the study of Vadakkepuliyaambatta et al. (2015) in the Barents Sea, canyon migration cannot not only break the original MTD structure, but it can also impact the local heat distribution, which may lead to an increase in heat flow on the sides of the canyon walls. Therefore, due to the minimal impact from later canyon activity, the pressure-temperature balance of well-preserved MTDs fluctuate and has an impact on hydrate accumulation. However, when later canyon activity reworks MTDs, the original litho-static pressure and its corresponding heat flow distribution may be changed, and the gas hydrate is more easily decomposed and released.

7.2 Effect of available water and gas resources

Available water provides a clathrate molecule skeleton; therefore, an adequate amount of free water is required within pores to effectively form hydrates. However, excess available water in pores may occupy spaces between free gases and have a negative impact on hydrate accumulation. In addition, Handa (1990) found that a suitable matching relation between available water and the gas source is crucial for enabling a hydrate synthesis reaction. In pattern AM.1, abundant gas sources are provided from the bottom gas chimney, and the well-preserved MTDs provide a suitable storage space and available water. Furthermore, the fine-grain seal above the MTD acts as a seal that stops free gas diffusion, and thereby provides enough refection time between the methane gas and available water.

In patterns RM.1 and RM.2, the accumulation factors, such as gas sources, suitable storage space, and available water, are similar to those for AM.1. However, canyon-migration erosion and normal-fault dislocation are capable of breaking the original fine-grain layers above the MTD, thereby suggesting that it is difficult for gas hydrate refection over a longer time period.

7.3 Effect of later canyon migration

The three types of MTDs have relationships with canyon development and migration. Hence, the three corresponding pattern types have mutual transformations. For example, the flow action of later turbidities may lead to an unstable and unconsolidated ridge and the development of MTDs, and later geological movements may cause conversion between these three patterns. Later canyon migration leads to basement erosion and may increase the occurrence of normal MTD development. However, if the canyon migrates to a region where MTDs are developing, the AM.1 pattern may be converted into a RM.1 pattern. Furthermore, if canyon migration is limited and tractive current developments, fine sediment (sedimentary wave or levee) may cover the reservoir and serve as a seal for free gas, which may then lead to the conversion of RM. 1 and RM. 2 in to AM. 1.

8 Conclusions

Based on the analysis of the deep-water canyon system in GMGS-3, this paper describes three types of MTDs. Three patterns are summarized based on results of a core-log-seismic integration study and with respect to hydrate accumulation.

(1) Two hydrate-bearing layers are distinguished based on an

analysis of electronic log and a core sample. The upper layer is fracture-filling hydrate and the lower layer is fine-grain-filling hydrate. A saturation count of the hydrate was conducted and reflective characteristics of 3D seismic data were evaluated. The regions overwhelmed by BSR distribution fit well with the MTDs along the ridge.

(2) Through seismic data interpretation, three kinds of MTDs are classified in the new drilling area at Shenhua: well preserved MTDs, MTDs eroded by canyon migration, and MTDs dislocated by contemporaneous faults.

(3) Three types of patterns are proposed based on a comparison of the three types of MTDs and their relationships with hydrate accumulation. Results show that a fine-grained seal is the key to gas accumulation. With respect to canyon migration and normal faults, the primary structure of the MTD often breaks and layers are sealed. Sand and fine mud mutually overlap in a sandwich pattern, which is the ideal type of MTD for accumulating hydrates on the northern slope of the SCS.

References

- Alsop G I, Marco S, Weinberger R, et al. 2016. Sedimentary and structural controls on seismogenic slumping within mass transport deposits from the Dead Sea Basin. *Sedimentary Geology*, 344: 71–90, doi: [10.1016/j.sedgeo.2016.02.019](https://doi.org/10.1016/j.sedgeo.2016.02.019)
- Bangs N L B, Hornbach M J, Berndt C. 2011. The mechanics of intermittent methane venting at South Hydrate Ridge inferred from 4D seismic surveying. *Earth and Planetary Science Letters*, 310(1–2): 105–112, doi: [10.1016/j.epsl.2011.06.022](https://doi.org/10.1016/j.epsl.2011.06.022)
- Behresht J, Bryant S L. 2012. Sedimentological control on saturation distribution in Arctic gas-hydrate-bearing sands. *Earth and Planetary Science Letters*, 341–344: 114–127, doi: [10.1016/j.epsl.2012.06.019](https://doi.org/10.1016/j.epsl.2012.06.019)
- Boswell R, Frye M, Sheldner D, et al. 2012. Architecture of gas-hydrate-bearing sands from Walker Ridge 313, Green Canyon 955, and Alaminos Canyon 21: Northern deepwater Gulf of Mexico. *Marine and Petroleum Geology*, 34(1): 134–149, doi: [10.1016/j.marpetgeo.2011.08.010](https://doi.org/10.1016/j.marpetgeo.2011.08.010)
- Chen Duanxin, Wang Xiujuan, Völker D, et al. 2016. Three dimensional seismic studies of deep-water hazard-related Features on the northern slope of South China Sea. *Marine and Petroleum Geology*, 77: 1125–1139, doi: [10.1016/j.marpetgeo.2016.08.012](https://doi.org/10.1016/j.marpetgeo.2016.08.012)
- Clift P, Lin Jian, Barckhausen U. 2002. Evidence of low flexural rigidity and low viscosity lower continental crust during continental break-up in the South China Sea. *Marine and Petroleum Geology*, 19(8): 951–970, doi: [10.1016/S0264-8172\(02\)00108-3](https://doi.org/10.1016/S0264-8172(02)00108-3)
- Di Celma C. 2011. Sedimentology, architecture, and depositional evolution of a coarse-grained submarine canyon fill from the Gelasian (early Pleistocene) of the Peri-Adriatic basin, Offida, central Italy. *Sedimentary Geology*, 238(3–4): 233–253, doi: [10.1016/j.sedgeo.2011.05.003](https://doi.org/10.1016/j.sedgeo.2011.05.003)
- Gong Chenglin, Wang Yingmin, Zheng Rongcai, et al. 2016. Middle Miocene reworked turbidites in the Baiyun Sag of the Pearl River Mouth Basin, northern South China Sea margin: Processes, genesis, and implications. *Journal of Asian Earth Sciences*, 128: 116–129, doi: [10.1016/j.jseaes.2016.06.025](https://doi.org/10.1016/j.jseaes.2016.06.025)
- Han Jianhui, Xu Guoqiang, Li Yangyang, et al. 2016. Evolutionary history and controlling factors of the shelf breaks in the Pearl River Mouth Basin, northern South China Sea. *Marine and Petroleum Geology*, 77: 179–189, doi: [10.1016/j.marpetgeo.2016.06.009](https://doi.org/10.1016/j.marpetgeo.2016.06.009)
- Handa Y P. 1990. Effect of hydrostatic pressure and salinity on the stability of gas hydrates. *The Journal of Physical Chemistry*, 94(6): 2652–2657, doi: [10.1021/j100369a077](https://doi.org/10.1021/j100369a077)
- He Yunlong, Xie Xinong, Kneller B C, et al. 2013. Architecture and controlling factors of canyon fills on the shelf margin in the Qiongdongnan Basin, northern South China Sea. *Marine and Petroleum Geology*, 41: 264–276

- Holbrook W S, Hoskins H, Wood W T, et al. 1996. Methane hydrate and free gas on the Blake ridge from vertical seismic profiling. *Science*, 273(5283): 1840–1843, doi: [10.1126/science.273.5283.1840](https://doi.org/10.1126/science.273.5283.1840)
- Horozal S, Kim G Y, Bahk J J, et al. 2015. Core and sediment physical property correlation of the second Ulleung Basin Gas Hydrate Drilling Expedition (UBGH2) results in the East Sea (Japan Sea). *Marine and Petroleum Geology*, 59: 535–562, doi: [10.1016/j.marpetgeo.2014.09.019](https://doi.org/10.1016/j.marpetgeo.2014.09.019)
- Jeong T, Byun J, Choi H, et al. 2014. Estimation of gas hydrate saturation in the Ulleung basin using seismic attributes and a neural network. *Journal of Applied Geophysics*, 106: 37–49, doi: [10.1016/j.jappgeo.2014.04.006](https://doi.org/10.1016/j.jappgeo.2014.04.006)
- Lee M W, Collett T S, Lewis K A. 2012. Anisotropic models to account for large borehole washouts to estimate gas hydrate saturations in the Gulf of Mexico Gas Hydrate Joint Industry Project Leg II Alaminos Canyon 21 B well. *Marine and Petroleum Geology*, 34(1): 85–95, doi: [10.1016/j.marpetgeo.2011.06.010](https://doi.org/10.1016/j.marpetgeo.2011.06.010)
- Li Gang, Yan Wen, Zhong Lifeng, et al. 2015. Provenance of heavy mineral deposits on the northwestern shelf of the South China Sea, evidence from single-mineral chemistry. *Marine Geology*, 363: 112–124, doi: [10.1016/j.margeo.2015.01.015](https://doi.org/10.1016/j.margeo.2015.01.015)
- Malinverno A. 2010. Marine gas hydrates in thin sand layers that soak up microbial methane. *Earth and Planetary Science Letters*, 292(3–4): 399–408, doi: [10.1016/j.epsl.2010.02.008](https://doi.org/10.1016/j.epsl.2010.02.008)
- Mitchum R M Jr. 1977. Seismic stratigraphy and global changes of sea level, Part 11, Glossary of terms used in Seismic Stratigraphy. In: Payton C E, ed. *Seismic Stratigraphy-Applications to Hydrocarbon Exploration*. USA: AAPG Memoir, 205–212
- Riedel M, Bahk J J, Kim H S, et al. 2013b. Seismic facies analyses as aid in regional gas hydrate assessments. Part-I: Classification analyses. *Marine and Petroleum Geology*, 47: 248–268
- Riedel M, Collett T S, Kim H S, et al. 2013a. Large-scale depositional characteristics of the Ulleung Basin and its impact on electrical resistivity and Archie-parameters for gas hydrate saturation estimates. *Marine and Petroleum Geology*, 47: 222–235, doi: [10.1016/j.marpetgeo.2013.03.014](https://doi.org/10.1016/j.marpetgeo.2013.03.014)
- Scholz N A, Riedel M, Bahk J J, et al. 2012. Mass transport deposits and gas hydrate occurrences in the Ulleung Basin, East Sea-Part 1: Mapping sedimentation patterns using seismic coherency. *Marine and Petroleum Geology*, 35(1): 91–104, doi: [10.1016/j.marpetgeo.2012.03.004](https://doi.org/10.1016/j.marpetgeo.2012.03.004)
- Sha Zhibin, Liang Jinqiang, Zhang Guangxue, et al. 2015. A seepage gas hydrate system in northern South China Sea: Seismic and well log interpretations. *Marine Geology*, 366: 69–78, doi: [10.1016/j.margeo.2015.04.006](https://doi.org/10.1016/j.margeo.2015.04.006)
- Shi Xiaobin, Qiu Xuelin, Xia Kanyuan, et al. 2003. Characteristics of surface heat flow in the South China Sea. *Journal of Asian Earth Sciences*, 22(3): 265–277, doi: [10.1016/S1367-9120\(03\)00059-2](https://doi.org/10.1016/S1367-9120(03)00059-2)
- Strozyk F, Huhn K, Strasser M, et al. 2009. New evidence for massive gravitational mass-transport deposits in the southern Cretan Sea, western Mediterranean. *Marine Geology*, 263(1–4): 97–107, doi: [10.1016/j.margeo.2009.04.002](https://doi.org/10.1016/j.margeo.2009.04.002)
- Vadakkepuliyambatta S, Hornbach M J, Bünz S, et al. 2015. Controls on gas hydrate system evolution in a region of active fluid flow in the SW Barents Sea. *Marine and Petroleum Geology*, 66: 861–872, doi: [10.1016/j.marpetgeo.2015.07.023](https://doi.org/10.1016/j.marpetgeo.2015.07.023)
- Wang Xiujuan, Collett T S, Lee M W, et al. 2014. Geological controls on the occurrence of gas hydrate from core, downhole log, and seismic data in the Shenhu area, South China Sea. *Marine Geology*, 357: 272–292, doi: [10.1016/j.margeo.2014.09.040](https://doi.org/10.1016/j.margeo.2014.09.040)
- Wang Xiujuan, Wu Shiguo, Lee W, et al. 2011. Gas hydrate saturation from acoustic impedance and resistivity logs in the Shenhu area, South China Sea. *Marine and Petroleum Geology*, 28(9): 1625–1633, doi: [10.1016/j.marpetgeo.2011.07.002](https://doi.org/10.1016/j.marpetgeo.2011.07.002)
- Wood W T, Hart P E, Hutchinson D R, et al. 2008. Gas and gas hydrate distribution around seafloor seeps in Mississippi Canyon, Northern Gulf of Mexico, using multi-resolution seismic imagery. *Marine and Petroleum Geology*, 25(9): 952–959, doi: [10.1016/j.marpetgeo.2008.01.015](https://doi.org/10.1016/j.marpetgeo.2008.01.015)
- Wu Nengyou, Zhang Haiqi, Yang Shengxiong, et al. 2011. Gas hydrate system of Shenhu Area, northern south China Sea: geochemical results. *Journal of Geological Research*, 2011: 370298
- Yu Xinghe, Wang Jianzhong, Liang Jinqiang, et al. 2014. Depositional characteristics and accumulation model of gas hydrates in northern South China Sea. *Marine and Petroleum Geology*, 56: 74–86, doi: [10.1016/j.marpetgeo.2014.03.011](https://doi.org/10.1016/j.marpetgeo.2014.03.011)
- Zhang Yi, He Lijuan, Wang Jiyang, et al. 2011. Heat flow pattern, base of methane hydrates stability zones and BSRs in Shenhu Area, northern South China Sea. *Acta Oceanologica Sinica*, 30(1): 59–67, doi: [10.1007/s13131-011-0091-x](https://doi.org/10.1007/s13131-011-0091-x)
- Zhou Wei, Wang Yingmin, Gao Xianzhi, et al. 2015. Architecture, evolution history and controlling factors of the Baiyun submarine canyon system from the middle Miocene to Quaternary in the Zhujiang River Mouth Basin, northern South China Sea. *Marine and Petroleum Geology*, 67: 389–407, doi: [10.1016/j.marpetgeo.2015.05.015](https://doi.org/10.1016/j.marpetgeo.2015.05.015)